Using air-coupled sensors to determine the depth of a surface-breaking crack in concrete

Seong-Hoon Kee and Jinying Zhu[a)]
Department of Civil, Architectural, and Environmental Engineering, The University of Texas, Austin, Texas 78712-0273

(Received 20 May 2009; revised 16 October 2009; accepted 31 December 2009)

Previous studies showed that the surface wave transmission coefficient across a surface-breaking crack in concrete can be used to estimate the crack depth. However, inconsistencies in the surface wave transmission measurements limit the test accuracy and application of this technique. The inconsistencies come from near-field scattering by the crack tip and inconsistent sensor coupling conditions on rough concrete surfaces. This study first investigates the near-field size based on numerical analyses, and then suggests that reliable surface wave transmission should be measured in the far field. Based on the far-field measurement, the relationship between the surface wave transmission ratio and the normalized crack depth (crack depth/wavelength) is obtained. In the experimental study, the air-coupled sensing method is proposed as a solution to the sensor coupling problem. Owing to the non-contact feature, the air-coupled sensing method not only improves testing speed but also enables more consistent signal measurement. The experimental study using air-coupled sensors shows good agreement with the results of numerical simulation and analytic solution. © *2010 Acoustical Society of America.* [DOI: 10.1121/1.3298431]

PACS number(s): 43.35.Pt, 43.20.Hq, 43.20.El [ADP] Pages: 1279–1287

I. INTRODUCTION

The early stage of damage in reinforced concrete structures generally begins with various types of surface cracks. The appearance of cracks on the concrete members may not necessarily imply structural failure; however, it causes many serviceability and durability problems, e.g., stiffness degradation, corrosion of the reinforcement bars, and infiltration of moisture and/or deleterious ingredients. These effects cause further deterioration and lead to the early malfunction of concrete structures. From the viewpoint of civil infrastructure sustainability, it is important to monitor the extent of cracks in reinforced concrete members to evaluate the deterioration level and, if necessary, to make appropriate rehabilitation decision.

Using nondestructive evaluation (NDE) methods to estimate the depth of a surface-breaking crack has been investigated extensively in recent decades. Previous studies showed that the surface (Rayleigh) wave transmission coefficient Tr across a surface-breaking crack can be used to estimate the crack depth. Using ultrasonic transducers, Viktorov (1967) experimentally developed the relationship between the Rayleigh wave transmission coefficient and the normalized crack depth h/λ, i.e., the ratio of crack depth to the wavelength for a surface-breaking crack in a solid. Achenbach and his colleagues (Achenbach *et al.*, 1980; Mendelsohn *et al.*, 1980; Angel and Achenbach, 1984) analytically derived the Tr and h/λ relation based on diffraction and scattering of harmonic incident Rayleigh waves by a surface-breaking crack in far field. Masserey and Mazza (2005) extended the analytical solutions by prior researchers (Achenbach *et al.*, 1980; Mendelsohn *et al.*, 1980) to an arbitrary excitation function and verified that the established Tr and h/λ relation by Achenbach *et al.* (1980) is also valid for arbitrary incident waves. Yew *et al.* (1984) experimentally verified the Tr and h/λ relation for cracks in aluminum specimens, in which the surface waves were generated by dropping a steel ball on the surface of a specimen. For concrete, a heterogeneous but globally isotropic material, the surface wave transmission (SWT) method has been proved sensitive to depth variation in surface-breaking cracks, even for tightly closed and ill-defined cracks (Hevin *et al.*, 1998; Popovics *et al.*, 2000; Song *et al.*, 2003; Shin *et al.*, 2008). Hevin *et al.* (1998) obtained the transmission ratio of a surface wave in the frequency domain using boundary element analysis, and proposed the cut-off frequency ($h/\lambda=0.3$) method to estimate a crack depth. Popovics *et al.* (2000) and Song *et al.* (2003) obtained the Tr and h/λ relation based on experimental study in laboratory. They found that the relationship is not affected by the width of the crack opening and the shape of crack tips. Figure 1 shows the surface wave transmission coefficient versus normalized crack depth curves developed by these researchers. Overall, these curves show a similar trend that Tr decreases with increasing h/λ, but differences between the curves are also obvious. For example, at Tr=0.6, the crack depths h/λ given by these four curves can vary from 0.19 to 0.33. To successfully apply the SWT method, a reliable Tr versus h/λ curve should be determined first. In this study, the authors attempted to explain the discrepancies among these curves proposed by the previous researchers. Then based on the conclusions, we proposed a practical and reliable surface wave transmission method for evaluating the crack depth.

The discrepancies in previous research may be explained by the near-scattering effects of surface waves due to inter-

a)Author to whom correspondence should be addressed. Electronic mail: jyzhu@mail.utexas.edu

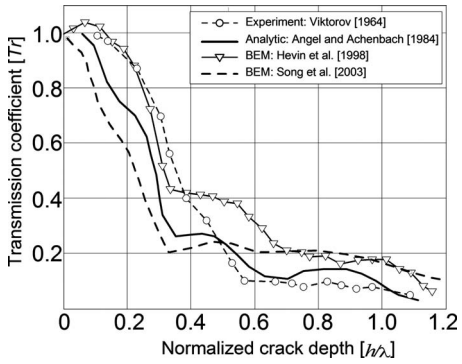

FIG. 1. Surface wave transmission coefficient versus normalized crack depth from previous literature.

action with the surface-breaking crack. Yew *et al.* (1984) observed that the signals measured in the near crack field were very complex due to the interference between surface waves and the bulk waves in the vicinity of a surface-breaking crack. Blackshire and Sathish (2002) investigated the near-field effect using a laser interferometer for a crack with $h/\lambda \gg 1$. They found that the signal amplitude at the crack location doubled the amplitude of the incident Rayleigh wave. The signal enhancement showed oscillatory variation in the vicinity of a surface-breaking crack and converged to a constant value when the measurement location is at a sufficiently far distance from the crack. Jian *et al.* (2007) studied the near-field scattering of the Rayleigh wave using numerical simulations [finite element method (FEM)]. In that investigation, they explained that the signal enhancement was mainly due to the interference effect of bulk waves (i.e., mode converted *P*- and *S*-waves in front of the crack, and bulk waves generated from the crack tip) and direct contribution of incident surface waves. Therefore, the surface wave transmission measurements will be affected by the near-field effect when the sensors are too close to the crack. In practice, however, the sensors cannot be placed too far from the crack (in true far field) due to dimension limit of the test specimen. This study investigated near-field effect variation with the sensor-to-crack spacing and proposed an approximate far-field sensor arrangement guideline.

In experiments, Achenbach *et al.* (1992) proposed a self-calibrating technique to reduce the experimental variability in surface wave measurement. The surface wave transmission ratios were measured from two opposite directions and averaged (the specific procedures are shown in the experimental section of this paper). This setup can eliminate effects of source variation and the coupling difference between two sensors, based on the assumption that coupling of the sensors during tests remains consistent (Popovics *et al.*, 2000). However, temporary sensor mounting methods, such as wax, adhesive, and magnetic mounts, will induce a low resonant frequency (usually below 10 kHz) which depends on the mounting stiffness of the contact sensors (e.g., accelerometers). The mounting resonant response affects the repeatability of tests. Poor signal consistency has been noticed in low frequency range by the authors and other researchers (Hevin *et al.*, 1998). The errors caused by this mounting resonance cannot be eliminated by the self-calibrating technique. On the other hand, permanent mounting cannot meet the requirement of rapid NDT tests and is difficult to apply to concrete. This study proposed a solution to this problem by using non-contact air-coupled sensors to improve test accuracy and efficiency.

Non-contact ultrasonic sensing techniques for concrete include air-coupled sensing and laser ultrasonic techniques. The laser technique has been shown effective to characterize Rayleigh wave attenuation in cement-based materials (Jacobs and Owino, 2000). However, the application of laser ultrasonic technique is still very limited in field testing due to expensive equipment and low reflection from rough surface of concrete. Air-coupled sensors have been successfully used to measure leaky surface waves in concrete by Zhu and Popovics (2005). Compared to contact sensors, the air-coupled sensors have the following benefits: (i) the non-contact sensing technique eliminates sensor coupling problems and thus gives more consistent measurement results; (ii) the non-contact feature enables rapid scanning of large civil engineering structures. To improve signal quality and test efficiency, this study combines the air-coupled sensing with the self-calibrating setup in surface wave transmission measurements.

This study first uses numerical simulations to investigate the parameters affecting surface wave transmission measurements, which includes the depth of crack h, impact duration of the source, and locations of sensors. An approximate far-field size is proposed. The Tr and h/λ relationship, based on measurements in the far field, is obtained. Then a simplified algorithm to calculate surface wave transmission coefficient is proposed in Sec. II E. In the experimental study, surface wave transmissions were measured from a series of notch-typed cracks in a concrete slab using air-coupled sensors. The experimental results validate the numerical results and show the promising application of air-coupled sensors.

II. NUMERICAL SIMULATION

A. FEM

The FEM was used to simulate the propagation behavior and near-scattering of surface waves caused by a surface-breaking crack in concrete. To save computational cost, a two-dimensional (2D) model was developed using rectangular quadratic axisymmetric elements (CAX4) in the commercial program (ABAQUS Inc., 2007). The validity of the model has been verified by Kim and Kwak (2008) to investigate properties of concrete using surface waves generated by a point impact source.

The model mesh size l_e and the time increment Δt for numerical integration procedure were carefully determined based on the wave velocity and frequency content (Ihlenburg, 1998). The mesh size was designed as 5 mm so that at least ten elements can participate to express the minimum wavelength λ_{min} in this study (Alleyne and Cawley, 1991). In this study, the λ_{min} for shear waves in concrete at f_{max} = 50 kHz is about 50 mm. The maximum time increment Δt for integration was determined as 1 μs, which is smaller than the characteristic time τ ($\tau = l_e/V_p$, where V_p is *P* wave velocity of concrete). Thus, a disturbance cannot propagate

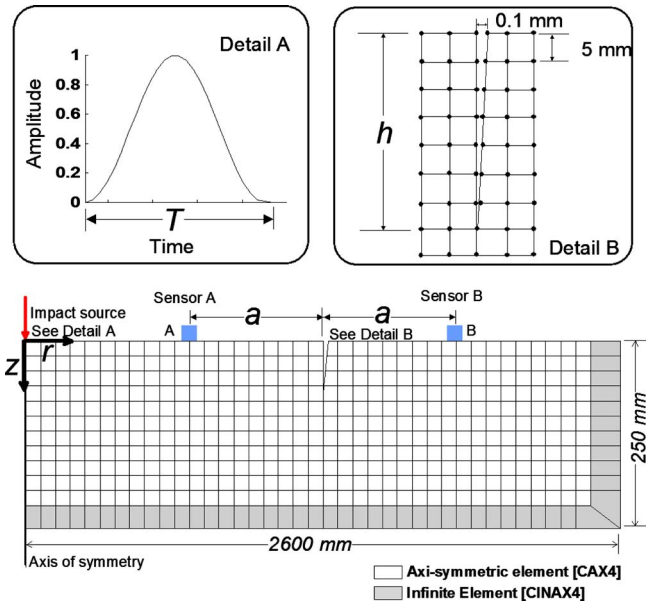

FIG. 2. (Color online) Finite element model for elastodynamic transient analysis in a solid half-space.

through a grid size during one time step. The finite element model is shown in Fig. 2. Sixteen models were analyzed for crack depth h ranging from 0 to 150 mm in a 10 mm step. To reduce wave reflections from boundaries, absorption boundary (CINAX4) elements were applied. The material properties are Young's modulus of 33 630 MPa, Poisson's ratio of 0.22, and mass density of 2400 kg/m^3. The corresponding velocities of P-, S-, and surface waves are 4050, 2420, and 2215 m/s, respectively. These material properties were chosen to simulate normal concrete.

A transient impact point source was applied on free-surface of the half-space at the axis of symmetry (i.e., $r=0$). The force function of the source is

$$f(t) = \begin{cases} \sin^2(\pi t/T), & 0 \le t \le T \\ 0, & t > T, \end{cases} \quad (1)$$

where T is the duration of impact. Note that the quadratic force function was selected to reduce Gibbs effect on FEM analysis (Kim and Kwak, 2008). The impact source is 1300 mm from the crack opening on the surface. To study the near-field effect caused by the crack tip scattering, various sensor locations on the surface of the concrete were investigated.

B. Near-field scattering of surface waves due to a surface-breaking crack

The size of near-scattering field around a crack depends on the crack depth and wavelength of the incident surface waves. Six numerical models, including two crack depths h =10 and 70 mm and four impact duration time T=40, 80 and 120 μs, were analyzed. These models correspond to six different h/λ of 0.12, 0.81, 0.06, 0.41, 0.04, and 0.27. Figure 3 shows the B-scan images of vertical velocity responses on the solid surface from the six models.

When h is much smaller than λ, e.g., h/λ=0.12 in Fig. 3(a), the dominant wave components are the reflected surface

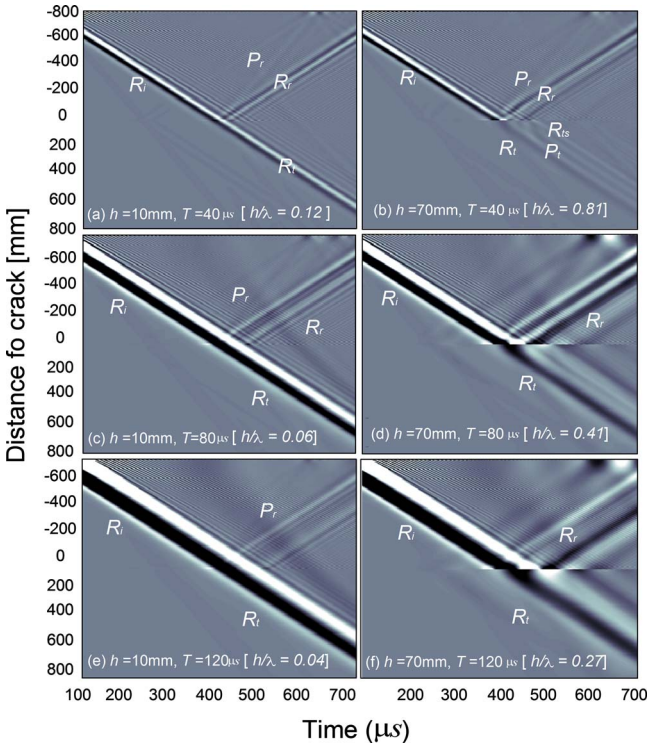

FIG. 3. (Color online) B-scan images of wave propagating on solid models with various h/λ: (a) 0.12, (b) 0.81, (c) 0.06, (d) 0.41, (d) 0.04, and (e) 0.27. (a)–(f) represent six models with two crack depths h=10 mm [(a), (c), and (e)] and 70 mm [(b), (d), and (f)], and three source duration times T =40 μs [(a), and (b)], 80 μs [(c), and (d)], and 120 μs [(e) and (f)].

waves (R_r) and the transmitted surface waves (R_t) after the incident waves (R_i) interact with the crack. The low frequency components of the surface waves can transmit through the crack, while most of high frequency components are reflected back by the crack. On the other hand, when $h/\lambda \sim 1.0$ (deep crack), most portions of the incident waves are reflected by the crack, as shown in Fig. 3(b).

In Figs. 3(a) and 3(b), the mode converted P-waves with a velocity of approximately 4000 m/s (P_r) are observed along with R_r. However, when the impact duration T increases to 80 and 120 μs, as shown in Figs. 3(c)–3(f), the mode converted bulk waves are not distinguishable from surface waves. Interferences between the incident and reflected surface waves are observed in the near region of the crack, as shown in Figs. 3(a) and 3(b). In addition to the reflected and transmitted surface waves, mode converted bulk waves and surface-skimming waves are generated by crack tip scattering.

C. Signal enhancement in the near field

Interaction between the mode converted waves (bulk waves, and multi-reflected waves) and the incident surface waves induces signal enhancement in the forward and backward scattering fields. This phenomenon has been noticed by Jian *et al.* (2007); however, the affected range (near-field size) was not studied in detail. In this paper, the authors present the signal enhancement around a crack and affecting parameters. For this purpose, the amplification coefficient (APC) is defined as the peak amplitude ratio between the

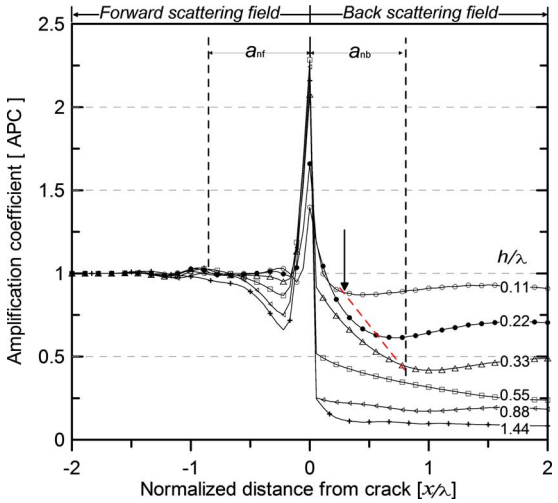

FIG. 4. (Color online) APC varies with the normalized distance from crack (x/λ) for different h/λ.

vertical displacements obtained on the cracked model (U_{zi}) and that on the crack free model (U_{z0}) as follows:

$$\mathrm{APC}(x/\lambda) = \frac{U_{zi}(x/\lambda)}{U_{z0}(x/\lambda)}. \tag{2}$$

APC was calculated for models of various impact durations T of 40–140 μs and crack depths h of 0 ~ 150 mm. Analysis based on the wide range of T and h shows that the APC depends on the distance from the crack x, the crack depth h, and the wavelength λ. Figure 4 shows amplification coefficient curves versus the normalized distance x/λ from the crack opening for various normalized crack depths (h/λ). In the backward scattering field, APC curves show very small oscillation (1%) when x is larger than 0.2λ. In the forward scattering field, APC curves decrease sharply from the upper peak at the location of the crack and then gradually reach a constant value with increasing x/λ. This constant value is the surface wave transmission coefficient in the far field.

Based on the results shown in Fig. 4, in the range of $h/\lambda = 0 \sim 1/3$, the approximate near-field size a_n measured from the crack opening can be expressed as

$$a_n/\lambda = 1.8h/\lambda + 0.1 \quad \text{for} \quad 0 \le h/\lambda \le 1/3. \tag{3}$$

Cheng and Achenbach (1996) suggested that $x/\lambda > 5$ can be approximately regarded as in the far field. However, this far-field requirement is difficult to satisfy in experiments due to the specimen size limit. Equation (3) is a less strict criterion, which provides a guideline to avoid significant signal enhancement. Surface wave transmission based on this criterion is slightly different from the curve built on far-field analysis (Angel and Achenbach, 1984), which will be shown in the following Sec. II D.

D. Calculation of transmission coefficient

The surface wave transmission function across a surface-breaking crack is defined as

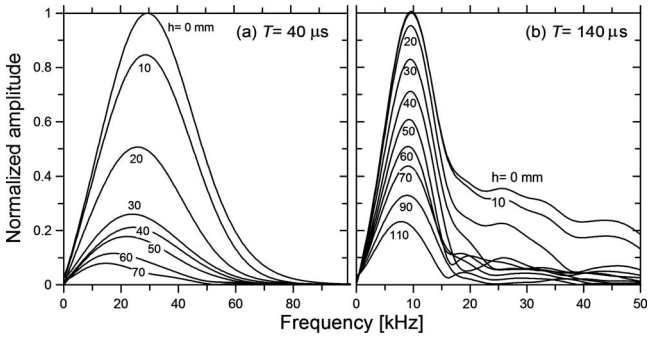

FIG. 5. Frequency spectra of windowed signals for various crack depths. The impact source duration times are (a) 40 μs and (b) 140 μs.

$$\mathrm{Tr}(f,h) = V_b(f,h)/V_a(f,h), \tag{4}$$

where Tr is the transmission coefficient in function of frequency and crack depth, and V_a and V_b are the Fourier transforms of the time domain signals measured at locations of A and B, respectively (Fig. 2). Sensors A and B are located in the far field based on the criterion in Eq. (3). To eliminate geometric attenuation effects, the transmission coefficient $\mathrm{Tr}(f,h)$ is normalized by the value obtained from a crack free model $\mathrm{Tr}(f,0)$.

Figure 5 shows the signal spectra $V_b(f,h)$ corresponding to impact source durations T of 40 and 140 μs, respectively, for crack depths h varying from 0 to 150 mm. A window function (a rectangular window) of three times of the impact duration $(3T)$ is applied to time domain signals to extract the transmitted surface wave signals. The figure shows that the center frequency f_c, the maximum amplitude, and spectral energy (area under the spectral curve) of the *transmitted surface waves* decrease with increasing crack depth h.

Figure 6 shows the normalized transmission coefficient Tr_n versus h/λ relationship when sensors are located at 650 mm $(\sim 5\lambda)$ from the crack opening. The sensors are in far-field region, according to Cheng and Achenbach (1996). The data in Fig. 6 were obtained from models with T=60 μs (center frequency of 17 kHz) and h from 0 to 100 mm. To investigate the effect of Poisson's ratio υ, transmission curves for υ of 0.2 and 0.3 were calculated. The results are shown as lines with open squares and open circles in Fig. 6,

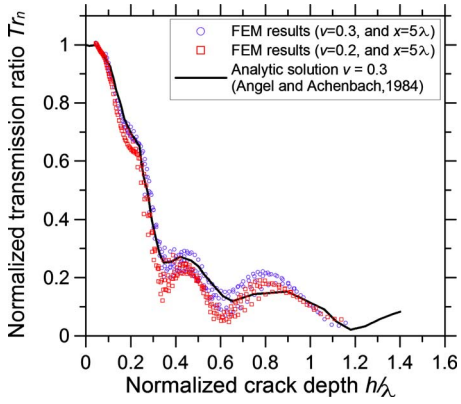

FIG. 6. (Color online) Normalized transmission coefficient versus normalized crack depth relation based on FE models and the analytic solution in far-field regions.

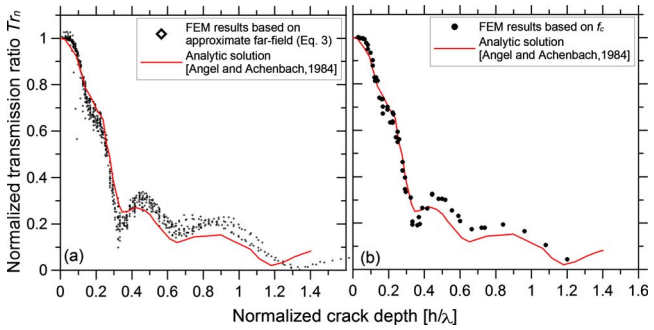

FIG. 7. (Color online) Normalized transmission coefficient versus normalized crack depth relation based on FE models in the approximate far-field region. The far-field analytic solution is also shown.

respectively. For comparison purposes, the analytical result given by Angel and Achenbach (1984) for v of 0.3 is also shown as solid line in Fig. 6. The transmission curve for $v=0.3$ shows good agreement with the analytical curve, which validate the numerical analysis models used in this study. Figure 6 also shows that Poisson's ratio has slight effect on the transmission function, but it is insignificant compared to other critical factors (h, x, and λ).

Figure 7(a) shows the Tr_n and h/λ relationship based on FEM models with T from 40 to 140 μs and h from 0 to 150 mm. The sensors are located in the approximate far-field region given by Eq. (3). For example, for $T=60$ μs and $h=50$ mm, the sensor location x was 110 mm ($a_n \sim 103.5$ mm with $\lambda \sim 135$ mm for $T=60$ μs). Overall, the data in Fig. 7(a) indicate that the FEM results agree with the analytic curve well, especially in the range of $h/\lambda=0 \sim 1/3$. Scattering of FEM data may come from two aspects: different Poisson's ratio (0.22 versus 0.3) and near-field effects. The criterion given by Eq. (3) is just an approximation to the true far field. Nevertheless, the data scattering has been significantly decreased when it is compared with previous research without considering near-field effects (Hevin *et al.*, 1998). The near-field effect may be a possible reason why the transmission curves obtained by other researchers (Song *et al.*, 2003) are different from the analytical results.

E. Simplified algorithm

The crack depth can be estimated by inversion process of the measured surface wave transmission function based on the established transmission curve. Reliable surface wave transmission measurements are the key to accurate evaluation of the crack depth. Figure 5 shows that a signal has the highest energy at the center frequency. Therefore, measurements around the signal center frequency may provide the most reliable results. Based on this assumption, we proposed a simplified algorithm to calculate the surface wave transmission. Instead of calculating wave transmission for all frequencies, we calculated Tr at the center frequency only. Then Eq. (4) is modified to

$$\mathrm{Tr}_n(f_c,h) = \mathrm{Tr}(f_c,h)/\mathrm{Tr}(f_c,0), \tag{5}$$

where f_c is center frequency of the input signal $V_a(f,0)$ (Fig. 5).

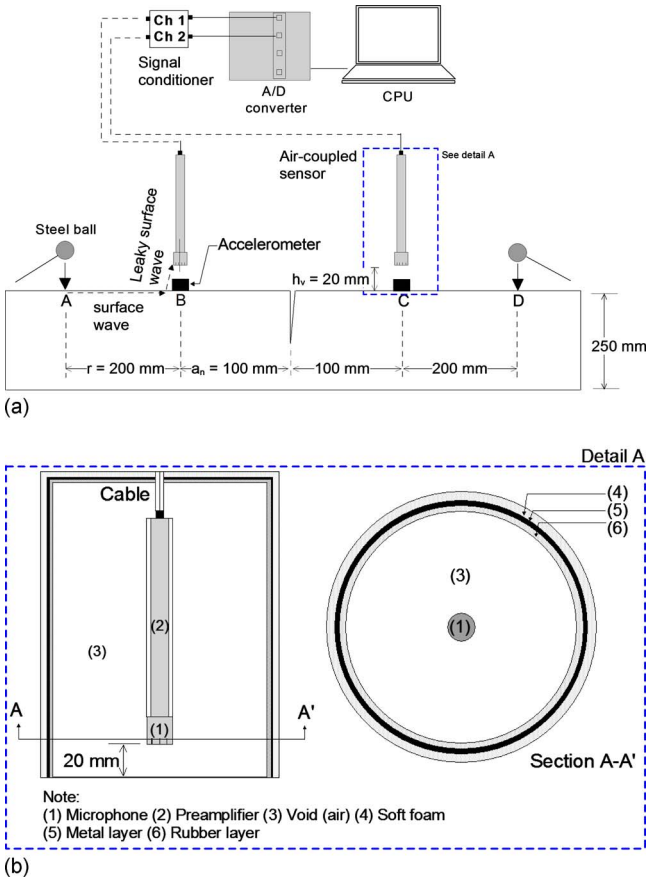

FIG. 8. (Color online) (a) Test setup based on self-compensation technique. (b) Detail of air-coupled sensor with sound insulation device.

With the measured surface wave transmission ratio at the center frequency, h/λ can be directly found from the established $\mathrm{Tr}_n \sim h/\lambda$ curve. If the surface wave velocity is known, the wavelength λ can be calculated, and then the crack depth can be determined. Figure 7(b) shows the $\mathrm{Tr}_n \sim h/\lambda$ curve based on measurements at center frequencies f_c. The impact source duration varies from 40 to 140 μs, and the crack depth h varies from 0 to 150 mm at 10 mm intervals. Good agreement is also observed between the center frequency measurement and the analytic solution, especially in the sensitive region where $h/\lambda \leq 1/3$.

III. EXPERIMENTAL VERIFICATION

A. Test setup

The surface wave transmission coefficient was measured for a notched concrete specimen using the air-coupled self-calibrating scheme. A schematic view of the test setup is shown in Fig. 8(a). Two air-coupled sensors were used to measure leaky surface waves propagating along the concrete surface. The air-coupled sensors (PCB model 377B01) have the following properties: nominal diameter of 6 mm, ±2 dB flat frequency response over 4 Hz to 80 kHz, and resonance frequency around 83 kHz. The horizontal spacing between the sensor and the impact source is designed as 200 mm to minimize the effects of direct acoustic waves. The sensor-to-crack spacing is 100 mm according to Eq. (3) to reduce near-field effects. According to Zhu and Popovics (2005), the

air-coupled sensors should be close to the test surface to reduce ambient noise and direct acoustic wave effects. In this study, the vertical distance between the sensors and the concrete surface h_v is 20 mm. Unlike a contact sensor, which measures waves right at the sensor location, an air-coupled sensor actually measures the surface waves emitting from the concrete surface at a distance of $h_v \tan\theta$, where θ is the leaky angle determined by Snell's law. This distance is defined as shadow zone. When this value is large, sensor locations should be corrected for shadow zone. In this study, the shadow zone size is about 3.0 mm, which is very small compared to the sensor to crack spacing at 100 mm.

To further reduce effects of direct acoustic waves and ambient noise, the air-coupled sensor was shielded by a sound insulation device, as shown in Fig. 8(b) (Zhu and Popovics, 2005).

A 250 mm thick concrete slab was cast in the laboratory. The thickness of the slab is larger than the wavelength of surface waves used in this study, so that the slab can be approximately regarded as a half-space, as assumed in the analytical and numerical models. Notch-type cracks with depth varying from 10 to 100 mm were generated in the specimen by inserting a 0.5 mm thick metal sheet before casting concrete. The metal sheet was removed from the concrete 12 h later. The width of the notches was measured by a crack width gauge, and it is about 0.5 mm. So the width-to-depth ratio of the notches used in this study is smaller than 0.1. According to Masserey and Mazza (2005), narrow slots with width-to-depth ratio smaller than 0.1 can be regarded as a crack, so that results from experimental study may be directly comparable with the theoretic results. The concrete was made from normal Portland cement type I/II, river sand, and gravel with a maximum size of 10 mm. The density of concrete is 2350 $\mathrm{kg/m^3}$, which was measured from five concrete cylinders (diameter of 10 cm and height of 20 cm), cast at the same time with the concrete specimen. The phase velocity of surface waves was calculated from a dispersion curve using the multichannel analysis of surface waves method (Ryden and Park, 2004). The velocity converged to 2200 m/s when the frequency is greater than 10 kHz. The velocities of *P*- and *S*-waves measured by low frequency ultrasonic transducers (50 kHz) in a through transmission mode were 4100 and 2460 m/s, respectively.

B. Data acquisition

The self-calibrating technique was used to measure surface wave transmission across the notch in concrete. The test setup is shown in Fig. 8(a). First, surface waves generated by an impact load at location A were recorded by sensors at locations B and C. The signals are denoted as V_{AB} and V_{AC}. Consequently, the wave transmission between locations B and C can be calculated from these two signals and denoted as T_{BC}. To eliminate the unsymmetrical effect caused by sensor coupling, an impact load is then applied at location D, and the signals recorded by the sensors at locations B and C are denoted as V_{DB} and V_{DC}. The transmission ratio between locations C and B is defined as T_{CB}. The average surface wave transmission function is (Popovics *et al.*, 2000)

$$|T_{BC}(f)| = \left| \sqrt{\frac{V_{AC}V_{DB}}{V_{AB}V_{DC}}} \right|. \tag{6}$$

To improve signal consistency, five repeated signal data sets were collected at the same test location. These five transmission functions were then arithmetically averaged in frequency domain. The signal coherence function shown in Eq. (7) was used to evaluate the consistency of obtained signals

$$SC_{BC}(f) = \frac{\left|\sum G_{BC}(f)\right|^2}{\sum G_{BB}(f) \times \sum G_{CC}(f)}, \tag{7}$$

where $G_{BC}(f)$, $G_{BB}(f)$, and $G_{CC}(f)$ are the cross spectrum and autospectrum functions between V_{AB} and V_{AC}, respectively. Similarly, $SC_{CB}(f)$ can also be calculated from signals V_{DB} and V_{DC}. The averaged $SC(f)$ is defined as

$$SC(f) = SC_{BC}(f)SC_{CB}(f), \tag{8}$$

which ranges from 0 to 1.0. A value close to 1.0 indicates good signal quality and repeatability. Therefore, the signal coherence function can be used to select the acceptable frequency range of a transmission ratio curve.

The measured surface wave transmission ratio Tr was further normalized by Tr_0, which is the transmission ratio obtained from a crack free region. This procedure will eliminate the geometric effect caused by a point source. All analyses were performed in the frequency domain. A *Hanning* window was applied to the time domain signals to extract the surface wave components.

Three steel balls with different diameters (7, 12, and 14 mm) were used as impact sources. They generate incident surface waves with center frequencies around 25, 20, and 18 kHz. The acquired signals were digitized at a sampling frequency of 10 MHz using an NI-PXI 5105 oscilloscope.

C. Typical signal measured using air-coupled sensors

Figure 9 shows typical time domain signals measured by two air-coupled sensors. Figure 9(a) presents signals obtained from a crack-free region of the concrete specimen, where the incident waves were generated by a source with impact duration about 60 μs. The impact duration T was measured from the received time domain signals of surface waves. The direct acoustic waves were completely separated from the leaky surface waves. In Fig. 9(b), clear incident and transmitted surface waves were also obtained from the crack region (h=40 mm) of concrete. Then the surface wave components were extracted from the signals by using a Hanning window.

D. Air-coupled sensors versus accelerometers

For comparison purposes, two accelerometers (PCB model 352C65) were also installed on the concrete surface with wax, right below the air-coupled sensors at locations A and B, respectively (see Fig. 8). Figure 10 shows the surface wave transmission coefficient and signal coherence functions for signals obtained from the 40 mm deep crack region using microphones [Fig. 10(a)] and accelerometers [Fig. 10(b)].

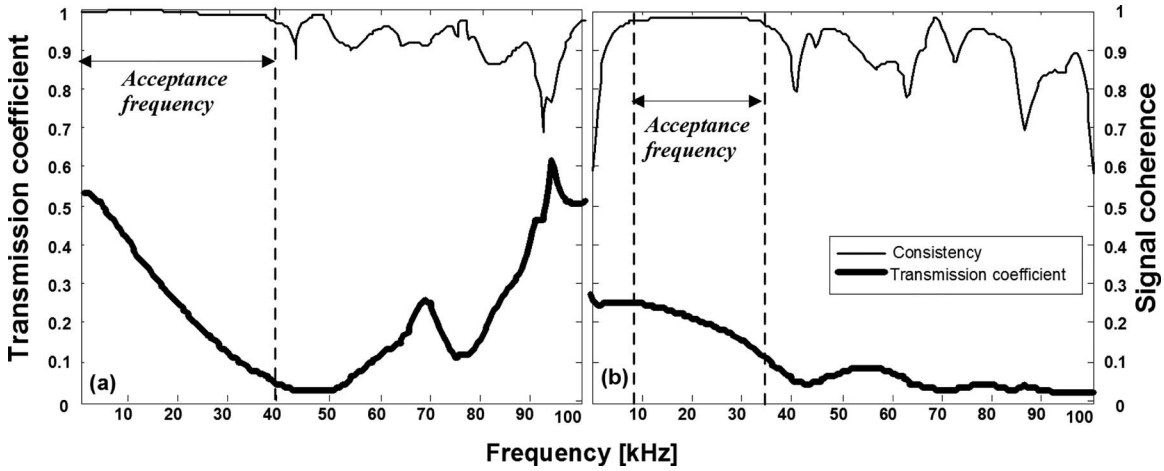

FIG. 9. Typical transmission coefficient and signal consistency versus frequency measured by (a) air-coupled sensors and (b) accelerometers. Depth of crack was 40 mm and the incident surface waves were generated by a 12 mm diameter steel ball.

The self-calibrating method was used in both tests. Both measurements show good coherence in the frequency range of 10–40 kHz. The upper limit of 40 kHz is governed by the frequency contents of the impact source. In the low frequency range (0–10 kHz); however, the air-coupled sensors show better coherence than the accelerometers. Although the accelerometers have flat frequency response in range 10–20 kHz, the temporary installation with wax causes strong resonant vibration at low frequency. This resonant vibration significantly affects signal quality around the resonant frequency, and the resonant effect cannot be removed by the self-calibrating procedure. When the center frequency of surface waves falls in this frequency range, the transmission coefficient will be unreliable. In field testing of concrete structures, the sensor coupling problem can be more critical due to rough surface of concrete and/or environmental conditions (e.g., dust, moisture, and temperature variation). Surface preparation is time consuming if large areas of concrete need to be tested. The air-coupled sensors provide a solution to this problem.

E. Calibration curve of transmission function using air-coupled sensor

The self-calibrating procedure was used to eliminate variation in the experimental setup (e.g., different impact sources, and difference between two sensors), and asymmetry in the tested specimen. Signal data were collected in the approximate far field for various crack depths with two air-coupled sensors. Three different steel balls of different diameters (7, 12, and 14 mm) were used to generate the incident surface waves. Surface wave transmission results from the three impact sources are shown in Figs. 11(a)–11(c). Overall, the experimental results show good agreement with the analytic solution, especially for shallow cracks, e.g., $h=20$ and 30 mm, and in the range of $h/\lambda<1/3$. The data corresponding to $h=10$ mm are not presented in this paper because a steel embedment under the crack distorted surface propagation. For deep cracks, the source should contain enough low frequency wave energy to give a reliable transmission measurement in $h/\lambda<1/3$ range. However, using long impact duration will induce boundary reflections from the back sur-

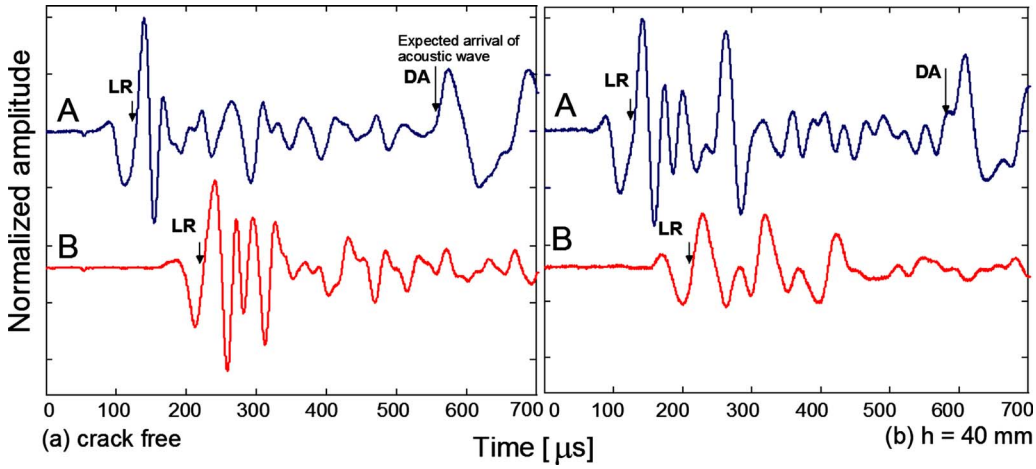

FIG. 10. (Color online) Typical signals measured by air-coupled sensors from a concrete specimen. The crack depths are (a) $h=0$ mm and (b) $h=40$ mm. The impact duration time is $T=60$ μs. Note that LR=leaky surface wave and DA=direct acoustic wave.

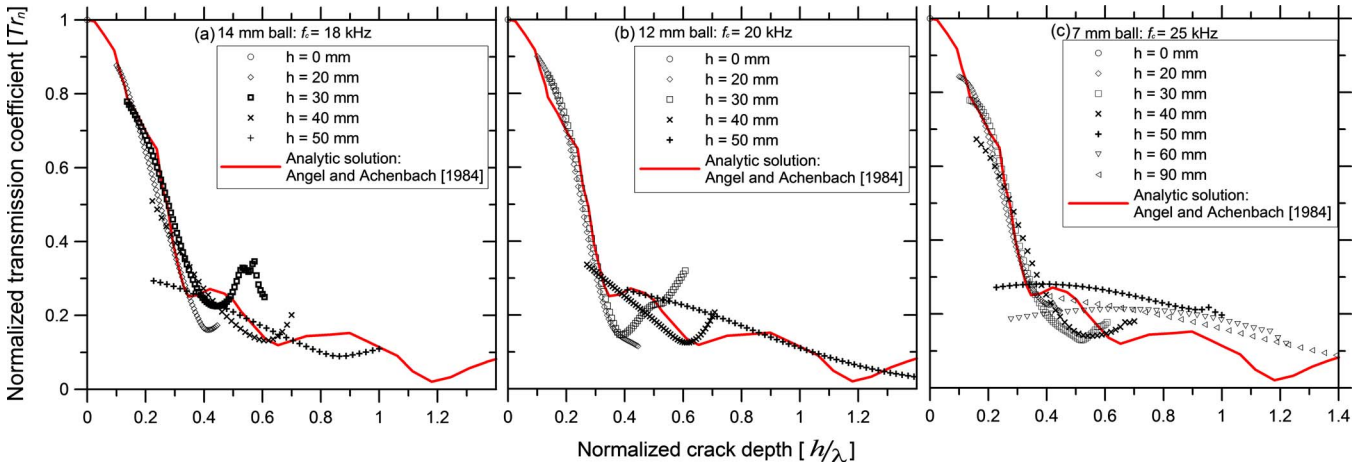

FIG. 11. (Color online) Normalized transmission coefficient and normalized crack depth relation.

face and stronger near-field effects. The crack depth that can be reliably measured using the surface wave transmission method depends on the impact source, sensor arrangement, and geometry (thickness and size) of the specimen. In this study, cracks up to 40 mm deep can be estimated with reasonable accuracy.

F. Experimental verification of the simplified algorithm using air-coupled sensor

To verify the proposed simplified algorithm for crack depth measurement, transmission coefficients measured at the center frequencies are shown in Fig. 12. The data are based on measurements at three center frequencies (18, 20, and 25 kHz) and crack depths (0, 20, 30, 40, 50, 60, and 70 mm). As shown in the figure, the experimental data are in good agreement with the analytic curve in $h/\lambda < 1/3$ range. The simplified algorithm provides a quick analysis of the measured surface wave transmission data to estimate crack depth.

IV. CONCLUSIONS

This study presents the surface wave transmission method to estimate the depth of a surface-breaking crack in concrete. First, this paper proposed a hypothesis that the near-field effect was the reason causing the discrepancy among previous research results. Numerical simulations were used to investigate the near-field effect caused by crack tip scattering and determined the near-field size. The surface wave transmission measured in the far field shows good agreement with the analytical solution, which verifies the proposed near-field effect hypothesis. Second, experimental studies were carried out on a concrete specimen to verify the numerical simulation results and demonstrate the effectiveness of the air-coupled sensing technique. The following conclusions are drawn based on the results of this study.

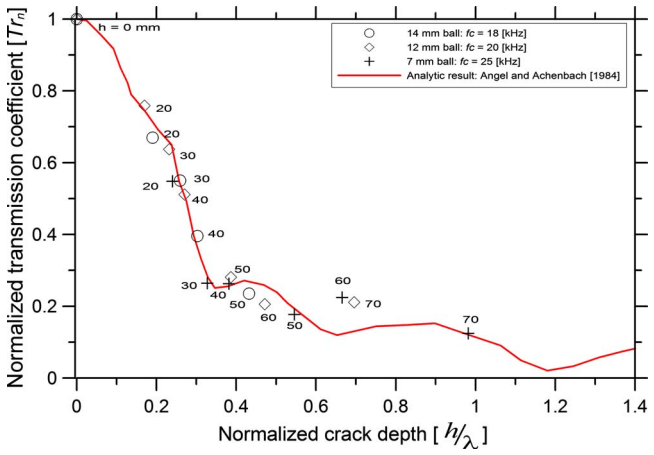

FIG. 12. (Color online) Normalized transmission coefficient based on center frequency and normalized crack depth relation.

(1) Surface wave transmission measurement is affected by near-field effects. To obtain reliable and consistent transmission coefficient, measurements should be performed in the far field. Analyses showed that the near-field size depends on the sensor location x, crack depth h, and an incident wavelength λ. An approximate near-field size [Eq. (3)] was proposed and verified effective to reduce the near-field effect in surface wave transmission measurements.

(2) The surface wave transmissions from FEM analyses and experimental studies show good agreement with the analytical curve given by Angel and Achenbach (1984). It verifies that the proposed test setup and signal processing procedure can be used to estimate of the depth of surface-breaking cracks in concrete, especially for small h/λ value ($h/\lambda < 1/3$).

(3) The air-coupled sensors show improved reliability and consistency in surface wave transmission measurements, as compared to the conventional contact sensors. Owing to the non-contact features, test speed is also improved.

(4) A simplified algorithm was proposed to estimate the crack depth based on the transmission value at the center frequency only, instead of trying to match the pre-established curve at all frequencies. If the surface wave velocity is known, the crack depth can be calculated at corresponding h/λ. The simplified algorithm has been verified by experimental data.

ABAQUS Inc. (**2007**). Analysis User's Manual, Version 6.7, Providence, RI.
Achenbach, J. D., Keer, L. M., and Mendelsohn, D. A. (**1980**). "Elastodynamic analysis of an edge crack," J. Appl. Mech. **47**, 551–556.
Achenbach, J. D., Komsky, I. N., Lee, Y. C., and Angel, Y. C. (**1992**). "Self-calibrating ultrasonic technique for crack depth measurement," J. Nondestruct. Eval. **11**, 103–108.
Alleyne, D., and Cawley, P. (**1991**). "A two-dimensional Fourier transform method for the measurement of propagating multimode signals," J. Acoust. Soc. Am. **89**, 1159–1168.
Angel, Y. C., and Achenbach, J. D. (**1984**). "Reflection and transmission of obliquely incident Rayleigh waves by a surface-breaking crack," J. Acoust. Soc. Am. **75**, 313–319.
Blackshire, J. L., and Sathish, S. (**2002**). "Near-field ultrasonic scattering from surface-breaking cracks," Appl. Phys. Lett. **80**, 3442–3444.
Cheng, A., and Achenbach, J. D. (**1996**). "A roller device to scan for surface-breaking cracks and to determine crack depth by a self-calibrating ultrasonic technique," Res. Nondestruct. Eval. **7**, 185–194.
Hevin, G., Abraham, O., Petersen, H. A., and Campillo, M. (**1998**). "Characterization of surface cracks with Rayleigh waves: A numerical model," NDT Int. **31**, 289–297.
Ihlenburg, F. (**1998**). *Finite Element Analysis of Acoustic Scattering* (Springer-Verlag, New York).
Jacobs, L. J., and Owino, J. O. (**2000**). "Effect of aggregate size on attenuation of Rayleigh surface waves in cement-based materials," J. Eng. Mech. **126**, 1124–1130.
Jian, X., Dixon, S., Guo, N., and Edwards, R. (**2007**). "Rayleigh wave interaction with surface-breaking cracks," J. Appl. Phys. **101**, 064906.
Kim, J. H., and Kwak, H.-G. (**2008**). "Nondestructive evaluation of elastic properties of concrete using simulation of surface waves," Comput. Aided Civ. Infrastruct. Eng. **23**, 611–624.
Masserey, B. and Mazza, E. (**2005**). "Analysis of the near-field ultrasonic scattering at a surface crack," J. Acoust. Soc. Am. **118**, 3585–3594.
Mendelsohn, D. A., Achenbach, J. D., and Keer, L. M. (**1980**). "Scattering of elastic waves by a surface-breaking crack," Wave Motion **2**, 277–292.
Popovics, J. S., Song, W.-J., Ghandehari, M., Subramaniam, K. V., Achenbach, J. D., and Shah, S. P. (**2000**). "Application of surface wave transmission measurements for crack depth determination in concrete," ACI Mater. J. **97**, 127–135.
Ryden, N., and Park, C. (**2004**). "Surface waves in inversely dispersive media," Near Surface Geophysics, **2**, 187–197.
Shin, S. W., Zhu, J., Min, J., and Popovics, J. S. (**2008**). "Crack depth estimation for concrete structures using spectral energy transmission of surface waves," ACI Mater. J. **105**, 510–516.
Song, W., Popovics, J. S., Aldrin, J. C., and Shah, S. P. (**2003**). "Measurement of surface wave transmission coefficient across surface-breaking cracks and notches in concrete," J. Acoust. Soc. Am. **113**, 717–725.
Viktorov, I. A. (**1967**). *Rayleigh Waves and Lamb Waves—Physical Theory and Application* (Plenum, New York).
Yew, C. H., Chen, K. G., and Wang, D. L. (**1984**). "An experimental study of interaction between surface waves and a surface breaking crack," J. Acoust. Soc. Am. **75**, 189–196.
Zhu, J., and Popovics, J. S. (**2005**). "Non-contact imaging for surface-opening cracks in concrete with air-coupled sensors," Mater. Struct. **38**, 801–806.